Lava flow morphology at an erupting andesitic stratovolcano: a satellite perspective on El Reventador, Ecuador

Article

Published Version

It is advisable to refer to the publisher's version if you intend to cite from the work. See Guidance on citing.

CentAUR

Central Archive at the University of Reading

Reading's research outputs online

Lava flow morphology at an erupting andesitic stratovolcano: A satellite perspective on El Reventador, Ecuador

D.W.D. Arnold [a], J. Biggs [a,*], H.R. Dietterich [b], S. Vallejo Vargas [d], G. Wadge [c], P. Mothes [d]

[a] COMET, School of Earth Sciences, University of Bristol, Queens Road, Bristol BS8 1RJ, UK
[b] Alaska Volcano Observatory, US Geological Survey, Anchorage, Alaska, USA
[c] COMET, Department of Meteorology, University of Reading, Earley Gate, P.O. Box 243, Reading RG6 6BB, UK
[d] Instituto Geofísico, Escuela Politécnica Nacional, Quito, Ecuador

ABSTRACT

Lava flows pose a significant hazard to infrastructure and property located close to volcanoes, and understanding how flows advance is necessary to manage volcanic hazard during eruptions. Compared to low-silica basaltic flows, flows of andesitic composition are infrequently erupted and so relatively few studies of their characteristics and behaviour exist. We use El Reventador, Ecuador as a target to investigate andesitic lava flow properties during a 4.5 year period of extrusive eruption between February 2012 and August 2016. We use satellite radar to map the dimensions of 43 lava flows and look at variations in their emplacement behaviour over time. We find that flows descended the north and south flanks of El Reventador, and were mostly emplaced over durations shorter than the satellite repeat interval of 24 days. Flows ranged in length from 0.3 to 1.7 km, and the length of flows generally decreased over the observation period. We measure a decrease in flow volume with time that is correlated with a long-term exponential decrease in effusion rate, and propose that this behaviour is caused by temporary magma storage in the conduit acting as magma capacitor between the magma reservoir and the surface. We use the dimensions of flow levées and widths to estimate the flow yield strengths. We observe that some flows were diverted by topographic obstacles, and compare measurements of decreased channel width and increased flow thickness at the obstacles with observations from laboratory experiments. Radar observations, such as those presented here, could be used to map and measure properties of evolving lava flow fields at other remote or difficult to monitor volcanoes.

1. Introduction

Lava flows are a commonly observed feature at volcanoes across a wide range of tectonic settings and magma compositions (e.g. Walker et al., 1973; Hulme, 1974; Eichelberger et al., 1986; Cashman and Sparks, 2013; Cashman et al., 2013). While they are rarely a threat to human life, they can damage or completely destroy infrastructure in their path (e.g. Jenkins et al., 2017). Understanding how lava flows advance and behave is therefore crucial for hazard management at active volcanoes (e.g. Felpeto et al., 2001; Behncke et al., 2005; Favalli et al., 2009; Harris and Rowland, 2009; National Academies of Sciences Engineering and Medicine, 2017). There have been numerous studies investigating lava flow characteristics and the underlying controlling physics, however most of these studies focus predominantly on mafic flows, especially flows from Hawai'i and Etna, Italy (e.g. Walker et al., 1973; Wadge, 1978; Malin, 1980; Pinkerton and Wilson, 1994; Calvari and Pinkerton, 1998; Harris et al., 2007; Harris and Rowland, 2009; Cashman et al., 2013). In comparison, silicic flows are under-represented in the scientific literature, in part because they are less common than mafic flows and therefore there are fewer observations of active flows of andesitic or dacitic composition (Borgia et al., 1983; Farquharson et al., 2015; Harris et al., 2004; Navarro-Ochoa et al., 2002; Kilburn and Lopes, 1991; Fink et al., 1987; Cigolini et al., 1984).

Lava flow advance is controlled by the interaction of numerous factors, including lava effusion rate (e.g. Walker et al., 1973; Wadge, 1981), vent geometry (e.g. Fink and Griffiths, 1992), underlying slope (e.g. Hulme, 1974; Gregg and Fink, 2000), topographical barriers (Dietterich and Cashman, 2014; Dietterich et al., 2015; Rumpf et al., 2018), and flow rheology (e.g. Hulme, 1974; Sparks et al., 1976; Fink and Griffiths, 1998; Kerr et al., 2006). As a natural function of this rheology, lava flows will form levées on the lateral margins of the

* Corresponding author.
E-mail address: Juliet.Biggs@bristol.ac.uk (J. Biggs).

flow, if the flow is active for a sufficiently long time (e.g. Hulme, 1974; Kerr et al., 2006). Levées have been observed on flows across the range of lava compositions and volcanic settings, as well as on the moon and Mars (Hulme, 1974; Sparks et al., 1976; Moore et al., 1978; Gregg and Fink, 2000; Harris et al., 2004; Chevrel et al., 2013). Lava flows can also form complex flow fields involving multiple, simultaneously active, branching channels (e.g. Lipman and Banks, 1987; Dietterich and Cashman, 2014). Branching can occur due to interaction with topographic obstacles (Dietterich et al., 2015), levée failure and overflow (Lipman and Banks, 1987), or pulses in lava supply rate (Bailey et al., 2006; Wadge et al., 2014; Keresaturi et al., 2016), and can dramatically affect the flow advance rate and maximum length (Dietterich and Cashman, 2014).

Remote sensing techniques provide a flexible method of tracking lava flow emplacement, even at remote or poorly accessible volcanoes (Sparks et al., 2012; Pyle et al., 2013). Numerous remote sensing methods have been used to monitor lava flow field development, including photogrammetry (e.g. Baldi et al., 2005; James et al., 2006), lidar (e.g. Favalli et al., 2010; Cashman et al., 2013), ground-, aerial-, and satellite-based optical and thermal surveys (e.g. Flynn et al., 1994; Harris et al., 2004; Kelfoun and Vallejo Vargas, 2015), and Synthetic Aperture Radar (SAR) (e.g. Smets et al., 2010; Ebmeier et al., 2012; Poland, 2014). By making repeat measurements of lava flow area and thickness it is possible to estimate lava volumes, as well as time-averaged discharge rates if the time interval between measurements is known (e.g. Harris et al., 2007). By comparing the extent of the lava flow at different times, it is also possible to make estimates of the lava flow front advance velocity and viscosity (e.g. Naranjo et al., 1992). Even for old lava flows that were emplaced without geophysical observations, detailed measurements of the morphology of the cooled flow can provide potential information about the flow viscosity, yield strength, and lava effusion rate (e.g. Pyle and Elliott, 2006; Deardorff and Cashman, 2012; Cashman et al., 2013).

1.1. El Reventador lava flows

To investigate the characteristics and behaviour of andesitic lava flow, we focus on recent lava flows extruded at El Reventador, Ecuador (Naranjo et al., 2016; Arnold et al., 2017). El Reventador is one of the most active volcanoes in Ecuador, with more than 20 historically observed eruptive periods since the 16th century (Simkin et al., 1981). The lava flows at El Reventador are basaltic-andesitic to andesitic in composition, with SiO_2 concentrations between 53 and 59% measured for flows erupted between 2002 and 2012 (Samaniego et al., 2008; Ridolfi et al., 2008; Naranjo, 2013). The solidified lavas from 2002 to 2009 have porphyritic textures, with between 20 and 35% phenocrysts by volume — mostly plagioclase, orthopyroxene and clinopyroxene, with minor amphibole, olivine and oxides (Naranjo, 2013). The analysed lava samples also contained between 10 and 40% vesicles by volume, with an average vesicularity of approximately 20% (Naranjo, 2013). Amphibole thermobarometry was used to determine that pre-2002, the reservoir was between 7 and 12 km deep and was periodically resupplied from below by pulses of volatile rich mafic magma (Ridolfi et al., 2008; Samaniego et al., 2008).

The post-2002 activity has been concentrated into five phases (A–E), lasting between one month and over 5 years, each separated by 18–24 months of relative quiescence (Naranjo et al., 2016; Wright, 2016). Between 2002 and 2009, 17 lava flows were extruded as part of Phases A–D and had a total lava volume range of 75 M to 90 M m³ (Naranjo, 2013; Naranjo et al., 2016), with Phase E starting with extrusion of a new lava flow on 9 February 2012. From the start of Phase E until 24 August 2016, a dense rock equivalent (DRE) of 44.8 M m³ of new lava was erupted at an average eruption rate of 0.31 ± 0.02 m³s⁻¹, although the effusion rate decreased approximately exponentially during this time (Arnold et al., 2017). Ground-based instruments that might indicate when flows are being actively extruded, such as seismometers or infrasound, are challenging to maintain in remote environments, and fieldwork to map flows can only be carried out infrequently. In this work, we build on the satellite radar observations of Arnold et al. (2017), which focused on the overall effusion rate, and investigate the individual lava flows in greater detail.

2. Data and methods

2.1. Radar amplitude

We use observations from radar and optical satellites to map lava flow emplacement at El Reventador between 2012 and 2016. Radar is an active remote sensing technique — the radar instrument transmits an electromagnetic signal at microwave frequency and receives the reflected signal. This active signal means observations can be made at night (unlike passive sensors at visible wavelengths), and the microwave frequencies are able to see through clouds, making radar an ideal tool for monitoring frequently cloudy volcanoes, such as El Reventador (e.g. Sparks et al., 2012; Pinel et al., 2014; Biggs and Pritchard, 2017). We use SAR observations from the Radarsat 2 and TanDEM-X satellite missions from 21 January 2012 to 24 August 2016 (Table 1).

The signal measured by a SAR sensor has an amplitude and phase component. The amplitude of a radar return is a function of the backscattered power from all reflectors within a pixel, which is a function of surface roughness at the length scale of the radar wavelength, the local slope relative to the satellite incidence angle, and the dielectric constant of backscatter material (e.g. Wadge et al., 2011). If the ground is resurfaced between two SAR acquisitions, then the backscatter properties of the resurfaced area will change. We can therefore observe new lava flows as a change in amplitude, which can be used to map the extents of flows (e.g. Wadge et al., 2012; Goitom et al., 2015). Due to decorrelation of radar phase measurements caused by rapid vegetation growth and explosive activity, it was not possible to accurately determine flow extents at El Reventador using SAR coherence mapping (Dietterich et al., 2012).

SAR images were processed using the Interferometric SAR Processor of the GAMMA software package (Werner et al., 2000). We

Table 1
SAR data used in this study.

Satellite	Orbit direction	Beam mode	Incidence angle/°	Number of scenes	Date range
Radarsat-2	Ascending	Wide 3	42	4	21 Jan. 2012–20 Jul. 2012
Radarsat-2	Descending	Ultrafine 25 Wide 2	48	25	06 Mar. 2012–24 Aug. 2016
TanDEM-X	Ascending	Experimental CoSSC	38	9	09 Sep. 2011–06 Jun. 2014
TanDEM-X	Descending	Experimental CoSSC	38	5	01 Jun. 2012–22 Jul. 2014

On ascending orbits, the satellite travels approximately south to north, looking to the east, while in a descending orbit, the satellite will travel approximately north to south, looking to the west.

co-registered each image to a single master image geometry and for each scene we created a Multi-looked Intensity (MLI) image with one range look to preserve maximum range resolution. MLI images were all geocoded using a digital elevation model (DEM) created from a TanDEM-X acquisition on 9 September 2011, to produce geocoded amplitude images with a horizontal pixel spacing of 2.5 m (Arnold et al., 2017). Geocoded images were imported into the QGIS software package for further analysis.

For each amplitude image we map the extent of flows that have been active since the previous image. We use the principle of superposition to determine relative ages if multiple flows have been active between acquisition dates. For each lava flow we determine the maximum down-flow length and flow area, as well as whether the flow formed levées and whether the flow was confined by topography. We also use the radar shadow width to estimate the thickness of the flow edge — where a topographic feature is steeper than the SAR incidence angle, that feature will cast a radar shadow, from which no signal is returned. The height of the object casting the shadow, h is given by

$$h = \frac{w_{los} \cos\phi}{\tan\theta} \tag{1}$$

where w_{los} is the shadow width in the direction of satellite line-of-sight, ϕ is the angle between the satellite line-of-sight and a line perpendicular to the edge of the lava flow and θ is the radar incidence angle (e.g. Wadge et al., 2011; Arnold et al., 2017). If we assume that the flows have a uniform thickness, then shadow estimates of the flow edge thickness can be used to estimate an average flow thickness, and hence flow volume when combined with the flow area. Lava volumes estimated from radar shadow widths were found to agree with independent volume estimates calculated from DEM differencing at El Reventador (Arnold et al., 2017), therefore assuming a constant flow thickness is an appropriate approximation in this case. For each flow, unless constraints are provided by additional data, we assume that the earliest possible start of lava extrusion is immediately after the last radar image (across all viewing geometries; Table 1) in which the flow does not appear, and the latest possible date of extrusion is the second before the earliest image after

which the flow does not advance any further. Taking these date limits gives a maximum time duration over which the flow could have been extruded, and therefore a minimum bound on the time-averaged discharge rate (TADR).

2.2. Height change maps

Newly emplaced volcanic deposits change the elevation of the land surface, which we can map by taking the difference between measurements of the topography acquired at different times (e.g. Wadge et al., 2006; Ebmeier et al., 2012; Dietterich and Cashman, 2014; Poland, 2014; Xu and Jónsson, 2014; Albino et al., 2015; Kubanek et al., 2015b; Kubanek et al., 2015a; Arnold et al., 2016; Naranjo et al., 2016). Areas that have significantly changed elevation between the DEM acquisition dates will appear as positive or negative height changes in the DEM difference map, which can be used to define the extent and thickness of lava flows. Unlike radar shadows, DEM difference maps can also be used to investigate thickness variations within a single flow, and to determine the thickness of other volcanic deposits, such as pyroclastic density currents and ash fall, that do not cast radar shadows and therefore cannot be measured by radar amplitude.

We use nine DEMs for El Reventador between 9 September 2011 and 6 June 2014 from ascending pass TanDEM-X scenes (Table 1), described more fully in Arnold et al. (2017). Each TanDEM-X scene consists of a pair of images, one from the TerraSAR-X satellite and the other from the TanDEM-X satellite, both acquired simultaneously from a single backscattered radar signal transmitted by one of the satellites. Since the satellites are separated in space, the path length from each satellite to the ground is different. This path length difference will appear as a relative phase difference, ϕ_{topo} between the two images, which is dependent on the height of the ground surface, z, and the perpendicular baseline distance between the two satellites, B_{perp}, and is given by

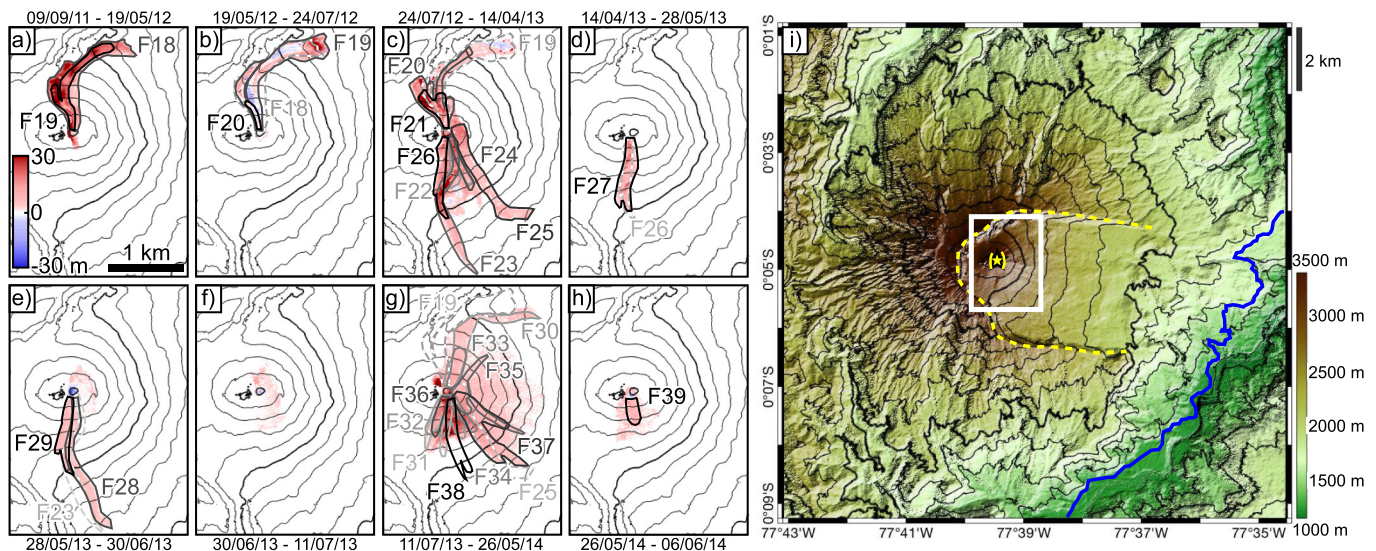$$z = \frac{r\lambda \sin\theta}{2\pi B_{perp}}\phi_{topo} \tag{2}$$

Fig. 1. Time series of height change maps between 9 September 2011 and 6 June 2014. Each map shows the elevation difference from the previous acquisition. Polygons show the outlines of flows that were active during each time interval, mapped from radar amplitude imagery. Positive elevation differences outside the mapped flow outlines are due to deposition of pyroclastic material during the given time interval. Dotted lines indicate flows that were active during a previous time interval and influenced the direction of travel of one or more flows in the shown time interval. Contours indicate the 2011 topography at intervals of 100 m with bold contours every 500 m. i) Hillshaded DEM of El Reventador. Contours indicate the 2011 topography at intervals of 200 m with bold contours every 1000 m. The white box shows the location of a)–h). The yellow star indicates the location of the summit lava dome. Solid yellow lines show the rim of the summit crater created by the 3 November 2002 eruption. The dashed yellow line follows the rim of the El Reventador crater. The solid blue line indicates the path of Ecuador State Highway 45 and approximate location of the trans-Andean oil pipeline.

where r is the range from the satellite to the ground surface and θ is the radar incidence angle and λ is the radar wavelength. We generate eight height change maps, by differencing consecutive DEMs (Fig. 1). The height change maps span time intervals ranging from 11 days (Fig. 1f and h) to 10 months (Fig. 1g).

3. Results

From radar amplitude imagery, we map 43 morphologically distinct lava flows that were active between 9 February 2012 and 24 August 2016. We number the flows 18–60 to distinguish them from those active during earlier phases of eruption. Detailed descriptions of each flow and time constraints on when they were active are provided in the supplementary material. The flows range in length from a few hundred metres to almost two kilometres (discussed in detail in Section 3.2.2), and have volumes of between 0.5 and 5 million m^3 (Table 2). The flows all appear to originate from the central summit lava dome, with no obvious activity from flank fissures or vents. Initially the direction of flow travel is confined by the 2002 summit crater, which directed flows to the north or south where the crater rim was breached. From 2014 onwards, the 2002 crater was infilled such that flows were able to overtop the eastern crater wall and travel down the east flank. The higher west crater wall was also partially overtopped in April 2015, allowing flows to descend to the northwest and southwest.

We observe several different types of flow morphologies and behaviour at El Reventador that are typical of viscous lavas. These are described in Section 3.1 and include simple unchannelised lava lobes, channelised flows that build levées of cooled lava, and branching flows, with multiple lobes or channels active simultaneously. We also note the effect of topographic confinement and obstacles on the dimensions and direction of travel of the flows, which are discussed in Section 3.1.3.

3.1. Case studies of emplacement conditions and dynamics

3.1.1. Levées and channels

We observe levées at 19 of the 43 flows, including 10 of the 12 flows greater than 1 km in length (Table 2). Assuming that flows behave as an isothermal Bingham fluid, the yield strength, Y, can be estimated from the height and width of the flows and levées (Hulme, 1974), given by

$$Y = h\rho g \sin\alpha \tag{3}$$

where h is the flow depth, ρ is the bulk density, g is the acceleration due to gravity and α is the slope of the base of the flow. If the flow has levées of width w, the yield strength is

$$Y = 2\rho g w \sin^2\alpha \tag{4}$$

and for a flow of width W,

$$Y = \frac{\rho g h^2}{W} \tag{5}$$

For lava flows that cool and crystallise as they are emplaced, the viscosity and yield strength are expected to increase as the flow cools and the isothermal approximation is therefore not valid (e.g. Kerr and Lyman, 2007). However, past work has shown that while mafic and long-lived eruptions may be strongly influenced by the growth of a surface crust or evolution in bulk rheology (e.g. Kerr and Lyman, 2007; Castruccio et al., 2014), isothermal models of flow advance with a constant yield strength perform well for andesite–dacite flows with blocky flow morphology and short-lived eruptions

(Castruccio et al., 2013; Kelfoun and Vallejo Vargas, 2015), equivalent to these El Reventador flows (Naranjo et al., 2016). Vallejo Vargas et al. (2015) report that Flow 38 was emplaced within 6 days, which is consistent with our observation that most flows at El Reventador are completely emplaced within the 24 day repeat period of Radarsat-2 measurements (Supplementary Material), and we therefore use the isothermal approximation.

We select three flows for which we have good TanDEM-X coverage (19, 25 and 28) and extract cross-sectional profiles for further analysis (Fig. 3). Flow 25 shows a clear anticorrelation between slope and flow/channel width. This relationship is less apparent for the other flows, likely due to the effects of flow branching, and diversion by topographical barriers (Fig. 3). We make additional measurements for Flow 38 using radar amplitude and the radar shadow method (Eq. (1)). Example flow cross section profiles are shown in Fig. 2 for Flow 19. By comparing DEMs generated from TanDEM-X images acquired before, during and after flow emplacement, we can accurately measure dimensions of the flow, and measure the slope of the pre-emplacement topography and compare how they change downhill (Table 3, Fig. 3).

We estimate the yield strength for the four flows using Eqs. (3)–(5) (Table 3). We find that there are significant differences in the yield strength estimated from levée morphology and overall flow morphology, with yield strength estimates between 8 and 232 kPa. These yield strength estimates are similar to those estimated for blocky dacitic flows at Santorini, Greece (Pyle and Elliott, 2006) and other andesitic flows (e.g. Lyman et al., 2004; Castruccio et al., 2013; Chevrel et al., 2013, 2016). Vallejo Vargas et al. (2015) used a 2–dimensional isothermal model of Bingham flow (Kelfoun and Vallejo Vargas, 2015) to fit thermal infrared camera observations of the advance rate of Flow 38, and found that the flow extent was well fit with a lava yield strength of 40 kPa and an effective bulk viscosity of 25×10^6 Pa s. Their yield strength of 40 kPa falls between our estimates from the levée thickness and flow width methods, suggesting that the yield strength for the other flows could lie in the suggested range. However, simulations of lava flow fields are very sensitive to yield strength and a parameter space over an order of magnitude could generate a wide range of possible outcomes.

3.1.2. Channel drainage

Once lava supply from the feeder vent stops, molten lava will continue to flow downhill causing a decrease in the lava level of active channels (e.g. Cigolini et al., 1984). We observe that levées often cast radar shadow or layover onto the channel between the levées, indicating that the height of the solidified levées exceeds the height of the main channel. The maximum levée height is formed during a period of high lava flux, while the main channel drains back below this level once the flux drops (e.g. Bailey et al., 2006; Wadge et al., 2014).

This effect was observed in Flow 19 in TanDEM-X images from 2012. The flow was active during the acquisition on 19 May 2012, but had stopped advancing by the subsequent acquisition on 24 July 2012. The height change map between these two dates shows an elevation decrease in the core of the flow, with elevation increases on either side (Fig. 1b). Profiles through the subsequent DEMs show increased height on the levées and decreased elevation in the channel for the upper 1300 m of the flow (Fig. 2b and c).

The increase in levée height between the two dates indicates that the flow in the channel reached a higher level than on 19 May 2012, possibly in one or more pulses of higher lava effusion rate (e.g. Bailey et al., 2006; Favalli et al., 2010; Wadge et al., 2012). After reaching this maximum highstand, the channel level dropped by up to 10 m below the 19 May height once extrusion at the summit ceased. The lava that drained from the channel accumulated at the flow front (Figs. 1b and 4), where the underlying slope dropped below 15°. At the flow front, Flow 19 exceeded 30 m thickness in places, which

Table 2
Flow parameters.

Flow	Earliest date dd/mm/yy	Latest date dd/mm/yy	Flow length[a] km	Flow area ×10⁵ m²	Flow volume ×10⁶ m³	Thickness m	Mean slope °	Initial flow bearing[b] °	Levées[c]	Topographic confinement[d]	Number of branches
18	09/02/12	18/05/12	1.68	3.71 ± 0.11	5.44 ± 0.83	14.7 ± 2.2	21.4 ± 8.4	352	X	X	2
19	12/04/12	24/07/12	1.75	3.39 ± 0.10	8.85 ± 0.72	14.3 ± 2.1	19.9 ± 7.7	341	X	X	2
20	10/06/12	14/09/12	1.20	2.02 ± 0.08	2.32 ± 0.36	11.5 ± 1.7	23.6 ± 7.1	343		*	4
21	24/07/12	14/09/12	0.58	0.97 ± 0.08	2.00 ± 0.35	20.4 ± 3.1	24.6 ± 2.5	339			2
22	17/08/12	14/09/12	0.82	1.52 ± 0.09	1.99 ± 0.32	13.1 ± 2.0	31.2 ± 4.9	160	X		2
23	14/09/12	20/01/13	1.69	1.68 ± 0.05	3.15 ± 0.48	18.7 ± 2.8	24.2 ± 7.0	159	X	*	1
24	20/10/12	20/01/13	0.75	0.85 ± 0.06	1.27 ± 0.21	14.9 ± 2.2	30.4 ± 5.4	161	X		1
25	22/01/13	25/03/13	1.55	1.93 ± 0.06	2.20 ± 0.34	11.4 ± 1.7	27.4 ± 7.2	099	X	*	1
26	29/01/13	25/03/13	1.13	1.49 ± 0.07	2.45 ± 0.38	16.4 ± 2.4	28.4 ± 5.7	195	X	*	2
27	14/04/13	28/05/13	0.91	1.20 ± 0.07	1.09 ± 0.17	9.0 ± 1.4	28.3 ± 6.3	193		*	2
28	28/05/13	30/06/13	1.71	1.94 ± 0.06	1.75 ± 0.27	9.0 ± 1.3	25.7 ± 7.2	174	X	X	1
29	05/06/13	30/06/13	0.92	1.31 ± 0.07	1.91 ± 0.30	14.5 ± 2.0	28.7 ± 4.8	197			2
30	11/07/13	09/09/13	1.77	2.23 ± 0.06	1.87 ± 0.28	8.3 ± 1.3	23.1 ± 9.6	010	X	X	1
31	23/07/13	09/09/13	0.89	1.67 ± 0.09	1.76 ± 0.28	10.5 ± 1.6	29.1 ± 3.3	186	X	X	3
32	09/09/13	14/12/13	0.55	2.01 ± 0.18	1.81 ± 0.32	9.0 ± 1.4	31.8 ± 5.3	191		X	4
33	14/12/13	07/01/14	0.49	0.78 ± 0.08	1.40 ± 0.25	18.1 ± 2.7	31.7 ± 2.4	019			1
34	14/12/13	07/01/14	0.62	0.69 ± 0.06	0.77 ± 0.13	11.1 ± 1.7	32.0 ± 4.5	139		X	1
35	07/01/14	20/03/14	0.97	1.51 ± 0.08	2.13 ± 0.34	14.1 ± 2.1	32.3 ± 5.4	092		*	3
36	31/01/14	20/03/14	0.53	0.68 ± 0.06	1.68 ± 0.30	24.7 ± 3.7	30.7 ± 4.2	209	X		1
37	20/03/14	13/04/14	1.22	2.75 ± 0.11	3.67 ± 0.57	13.4 ± 2.0	30.6 ± 5.5	126	X	X	3
38	20/03/14	17/05/14	1.19	2.02 ± 0.08	2.12 ± 0.33	10.5 ± 1.6	28.1 ± 6.3	166	X	*	2
39	26/05/14	06/06/14	0.32	0.38 ± 0.06	0.64 ± 0.14	16.8 ± 2.5	29.5 ± 4.0	168			1
40	08/06/14	21/06/14	0.90	1.36 ± 0.08	1.29 ± 0.21	9.4 ± 1.4	32.7 ± 3.2	156	X	*	2
41	18/07/14	28/09/14	0.61	0.94 ± 0.08	1.12 ± 0.19	11.9 ± 1.8	30.0 ± 2.4	147			2
42	22/10/14	09/12/14	0.47	0.34 ± 0.04	0.52 ± 0.10	15.2 ± 2.3	31.4 ± 5.1	004	X	*	1
43	22/10/14	09/12/14	0.92	1.30 ± 0.07	1.82 ± 0.29	14.0 ± 2.1	30.4 ± 5.5	215	X	X	2
44	09/12/14	26/01/15	0.44	0.58 ± 0.07	0.81 ± 0.15	13.9 ± 2.1	29.3 ± 2.3	201			1
45	26/01/15	19/02/15	0.33	0.42 ± 0.06	0.88 ± 0.19	21.0 ± 3.2	28.1 ± 2.6	339		X	2
46	26/01/15	19/02/15	0.67	0.96 ± 0.07	1.55 ± 0.26	16.3 ± 2.4	31.7 ± 2.8	215		X	2
47	19/02/15	15/03/15	0.30	0.43 ± 0.07	0.52 ± 0.12	12.3 ± 1.8	29.2 ± 2.0	178		*	2
48	15/03/15	06/08/15	1.13	0.72 ± 0.03	1.60 ± 0.25	22.3 ± 3.3	31.2 ± 4.9	042		*	1
49	15/03/15	06/08/15	0.63	0.67 ± 0.05	1.01 ± 0.17	15.2 ± 2.3	25.1 ± 3.4	304		X	1
50	15/03/15	06/08/15	1.09	1.30 ± 0.06	1.65 ± 0.26	12.7 ± 1.9	30.0 ± 4.3	160	X	X	1
51	15/03/15	06/08/15	0.60	0.62 ± 0.05	0.90 ± 0.15	14.5 ± 2.2	32.8 ± 3.3	213		*	1
52	15/03/15	06/08/15	0.57	0.86 ± 0.08	1.32 ± 0.23	15.3 ± 2.3	30.5 ± 2.4	155	X		1
53	15/03/15	28/08/15	0.92	0.56 ± 0.03	0.49 ± 0.08	8.8 ± 1.3	27.8 ± 6.3	002		*	1
54	23/09/15	30/10/15	0.88	0.83 ± 0.05	1.30 ± 0.21	15.7 ± 2.4	29.1 ± 3.4	359	X	X	1
55	17/10/15	03/02/16	0.61	0.94 ± 0.08	2.63 ± 0.45	28.1 ± 4.2	22.1 ± 5.4	322			1
56	11/01/16	03/02/16	0.60	0.44 ± 0.04	0.47 ± 0.08	10.7 ± 1.6	31.5 ± 3.5	127			1
57	18/01/16	02/04/16	0.61	0.67 ± 0.06	0.90 ± 0.15	13.4 ± 2.0	29.9 ± 2.3	217		X	1
58	02/04/16	31/07/16	0.51	0.39 ± 0.04	0.49 ± 0.09	12.6 ± 1.9	31.9 ± 3.0	033		X	1
59	31/07/16	13/08/16	0.50	0.33 ± 0.03	0.46 ± 0.08	14.0 ± 2.1	23.1 ± 4.3	288		X	1
60	13/08/16	24/08/16	0.64	0.83 ± 0.06	0.90 ± 0.15	10.8 ± 1.6	28.6 ± 5.0	358		X	3

[a] Uncertainties on all flow length measurements are ± 50 m.

[b] Bearing is the angle with respect to North. Uncertainties on all flow bearing measurements are ± 5°.

[c] X indicates that levées were present for at least part of the flow.

[d] X indicates that one edge of the flow was topographically confined for at least part of the flow, * indicates that both edges of the flow were topographically confined for at least part of the flow.

was the maximum TanDEM-X measured thickness attained by an individual flow.

The volume of lava that accumulated at the foot of Flow 19 between 19 May and 24 July 2012 was 0.98 ± 0.10 M m³, while the measured volume decrease in the channel for the same time interval was 0.33 ± 0.14 M m³. In order to match the volume at the flow front, the mean lava depth in the channel is calculated to have increased by 6.2 m before drainage, which matches well with the observed mean levée height increase of 6.3 ± 1.4 m between 19 May and 24 July 2012.

3.1.3. Interaction with barriers

Lava flows are currents that travel downslope under the force of gravity. Underlying topography strongly influences the path taken by lava flows, which will accelerate on steeper slopes and can be diverted or split by topographical barriers (e.g Dietterich and Cashman, 2014; Dietterich et al., 2015, 2017). When a flow travelling downhill impacts with a barrier, the flow upslope of the barrier will

thicken and, depending on the angle between the flow and the barrier, the flow advance rate can either increase or decrease (Dietterich et al., 2015).

We observe numerous flows at El Reventador where the flow path is either partially or entirely controlled by interaction with pre-existing topographic barriers. These barriers include the large ∼ 200 m high wall of the horseshoe-shaped crater that surrounds the El Reventador stratocone (e.g. Flows 18 and 19, Fig. 5a), the east and west walls of the 2002 summit crater (e.g. Flows 25 and 35, Fig. 5c), fluvially incised gullies radiating away from the stratocone summit (e.g. Flows 35 and 48, Fig. 5d) and the sides and levées of previously emplaced lava flows (e.g. Flows 20, 28, and 30, Fig. 5b).

While many flows are topographically confined, our data best capture the local effects of flow interaction with a topographic barrier for Flow 19. This flow encountered the northern wall of the El Reventador crater at a down-flow distance of 700 m from the summit, diverting the channel at an angle of ∼35° (Fig. 2). The diversion caused a rerouting of the flow to a path that has a decreased slope (5°), resulting in a decrease in channel width of ∼20 m, and
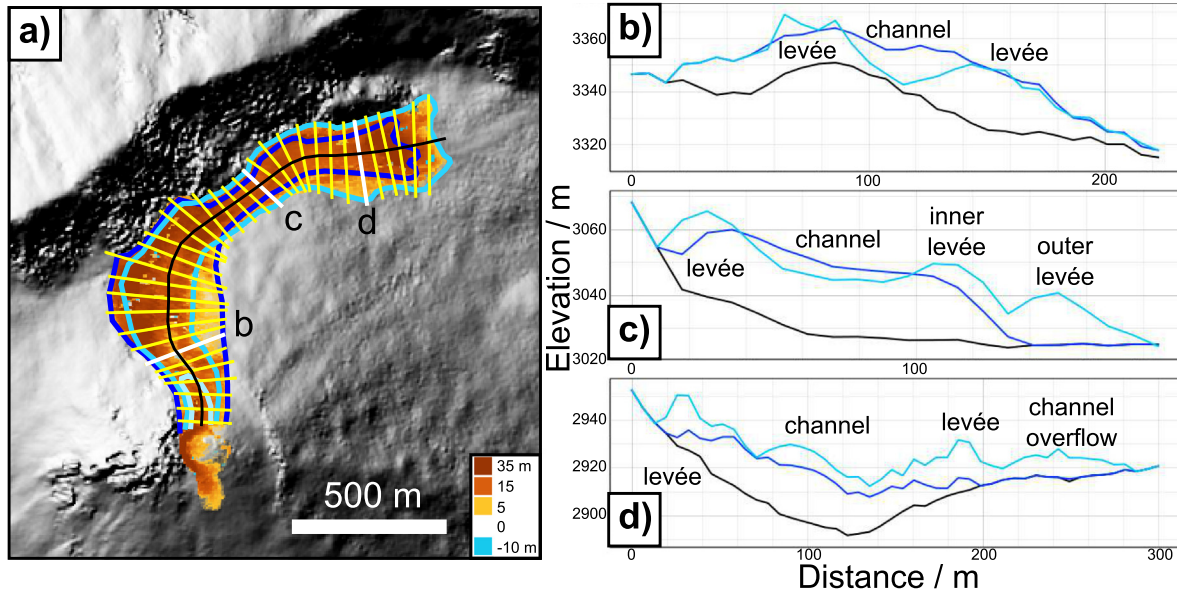
Fig. 2. a) Map of Flow 19, which we use to estimate the yield strength of lava flows at El Reventador. Flow heights represent topographic change between 9 September 2011 and 24 July 2012, and include Flows 18 (dark blue), 19 (light blue) and part of 20 (light green). The black line indicates the centre line of Flow 19 used in Fig. 4. Cross section lines are every 50 m down the flow channel and are used to estimate flow thickness, flow width, levée width and channel width. b), c), and d) Cross section profiles through Flows 18 and 19. The black lines give pre-Phase E topography on 9 September 2011, the dark blue lines give topography on 19 May 2012, when Flow 18 had been completely extruded and Flow 19 was still active, and light blue lines show topography on 24 July 2012, when Flow 19 had been completely emplaced. The black dotted line gives the approximate location of the top of Flow 18 (and therefore base of Flow 19).

an increase in flow thickness of ~5 m (Fig. 3). These changes in morphology with obstacle interaction are comparable to the results of analogue experiments with similar geometry (Dietterich et al., 2015), with implications for flow dynamics. The thickening of the flow against the obstacle reflects the formation of a bow wave upslope where incoming lava builds up head to divert along the barrier (Dietterich et al., 2015). The observed change in thickness (quantified as the ratio between pre- and post-barrier thickness) is ~1.3. This is smaller than that observed for equivalent geometries in experimental golden syrup and molten basalt flows (1.9—2.6), suggesting that the lower advance rate (0.3 mm s^{-1} compared to 1.1–3.3 mm s^{-1}) and greater viscosity of Flow 19 relative to the experimental flows (10^7 Pa s compared to 10^2 Pa s) reduces bow wave formation. The experimental results suggest that flow thickening combined with narrowing against the obstacle in this geometry would have accelerated flow advance along the crater wall, despite the reduced slope along the flow path (Dietterich et al., 2015).

3.1.4. Branching

Lava flows often split into multiple branches, which can be active at the same time (e.g. Dietterich and Cashman, 2014). We observe that 20 out of 43 flows at El Reventador had more than one active branch. The maximum number of branches for a single flow was 4 (Flows 20 and 32), however we do not see complex bifurcation networks that have previously been observed at large basaltic and andesitic flows (Lipman and Banks, 1987; Deardorff and Cashman, 2012; Dietterich and Cashman, 2014).

Flows can either split at the flow front to branch around topographic obstacles (e.g. Favalli et al., 2005; Dietterich et al., 2015), or branches can form from a pre-existing channel, either through lava overflowing, or breaking through, the channel wall (e.g. Lipman and Banks, 1987; Bailey et al., 2006; Tarquini and Vitturi, 2014). We observe both of these behaviours in the El Reventador flows. For instance, Flow 20 has 4 branches (Fig. 5b), of which the central two were divided, and then confined, each by the levées of a branch of

Flow 19. In contrast, the eastern and western branches both over-topped the Flow 19 levées, and were able to spread laterally without confinement.

Once a flow has split in two, branches do not appear to recombine, even if they contact each other. For example, we observe that on 10 June 2012, the western branch of Flow 19 was diverted by the northern wall of the El Reventador crater into the levées of the eastern branch of Flow 19 (Fig. 5a). Since the flow front was laterally confined in all directions, the flow thickened until it was able to overtop the levée of the eastern branch and flow into the channel of the eastern branch. However in the subsequent image on 24 July 2012, the levées of the eastern channel of Flow 19 had significantly increased in height, and the channels had not recombined (Fig. 5b). We presume that the cool, solidified flow levées provide a thermal and rheological barrier that prevents the flow branches from merging. For basaltic lava flows, confinement by topographical barriers can cause flow channels to merge (Dietterich and Cashman, 2014). However, the time between flows at El Reventador is much greater than for the example of Kīlauea (merging of contemporaneous flow lobes), meaning the margins would have formed levées and cooled more, creating a rheological divide that prevented the flows combining.

We find that the number of branches per flow decreases with time over the observation period (Fig. 6b), and there is a similar trend with respect to the presence of levées (Fig. 6a). However, there is no correlation between flows having levées and flows having multiple branches. Of the 19 flows with levées, 9 have multiple branches and 10 have a single channel, while for flows without levées, the numbers are 11 and 13 respectively. In contrast to observations of basaltic lava flows on Hawai' i (Dietterich and Cashman, 2014), we do not find any correlation between underlying slope and the number of branches (Fig. 6c). Dietterich and Cashman (2014) hypothesised that the increased number of branches on steeper slopes was due to flows thinning and therefore branching around small topographical obstacles that would be overtopped on shallower slopes when the flows were thicker.
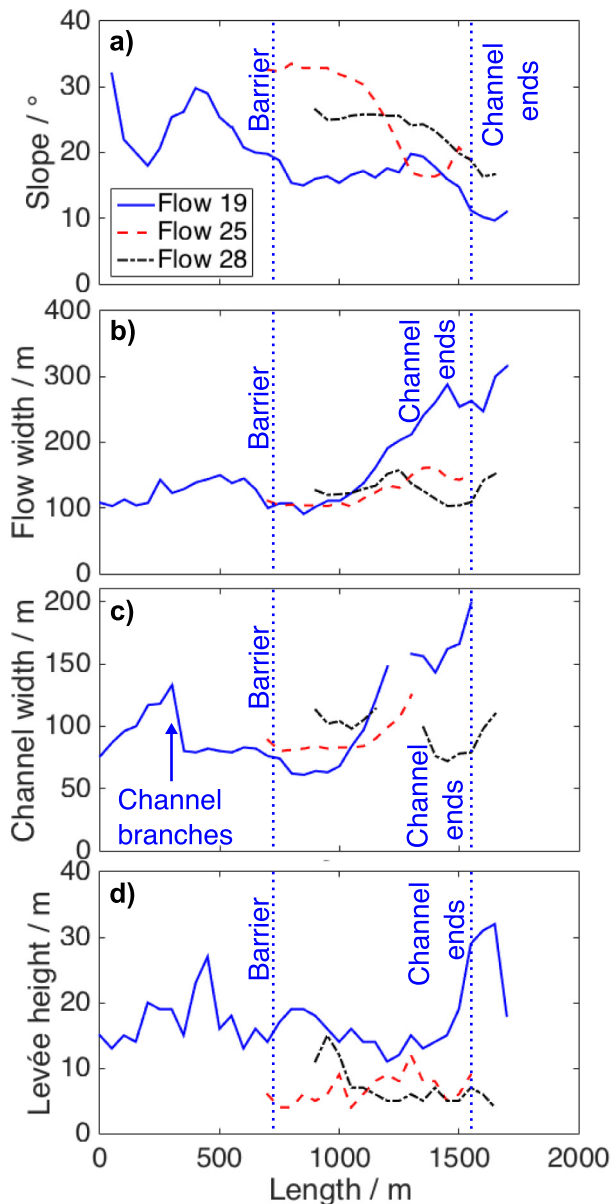
Fig. 3. Downslope variation of flow parameters for Flows 19 (solid blue lines), 25 (dashed red lines), and 28 (dot-dashed black lines). Flow 25 shows clear anticorrelation between slope and flow/channel width. This relationship is less apparent for the other flows, likely due to the effects of flow branching, and diversion by topographical barriers, which are labelled on the profile for Flow 19 where they have a clear impact. Note that in d, the values for the lower 300 m of Flow 19 represent the maximum flow thickness, rather than levée height.

That we do not observe similar behaviour is most likely because the flows at El Reventador are thicker than the Hawai'i flows, and therefore are able to overtop small obstacles even on steep

slopes. Branching is instead primarily caused by interaction with large scale obstacles, such as the edges of previously emplaced lava flows.

3.2. Overall parameters

3.2.1. Flow direction

The lava flows observed during Phase E almost exclusively descended the north or south flanks of El Reventador, following the pattern of previous phases (Naranjo et al., 2016). The direction of flow travel appears to be primarily determined by the geometry of the 2002 summit crater and the lava dome and cinder cone that were growing inside this crater. Fig. 7 shows that while flows were confined to travelling approximately north or south in 2012 to 2014, flows spread out more in 2015 and 2016. Since lava flows behave as gravity currents they will flow down the steepest local slope into topographic minima, however once the flow has solidified and the original topographic low has been infilled, future flows may follow a different route. At El Reventador, this results in flows extruded during 2015 and 2016 to advance in more easterly and westerly directions than those emplaced in earlier years, with a significant change in behaviour after January 2014, when the base of the dome reached the height of the eastern crater rim.

3.2.2. Flow dimensions

The flow length, area and volume all show a general decrease through time as the eruption progresses (Fig. 8). The flow lengths decreased from > 1.5 km in 2012 and 2013 to < 1 km in 2016. There is a strong correlation between flow length and topographic confinement — all flows > 1 km in length had levées and/or were either partially or wholly confined by topography. We observe a similar trend with flow area and volume, with the largest flows extruded earlier in the eruptive phase. In contrast there is no significant temporal trend in flow thickness. Average flow thicknesses vary between 8 and 28 m, and both the mean and median thickness of all flows are 14 m.

The length and area of lava flows are at least partially controlled by the lava effusion rate (e.g. Walker et al., 1973; Malin, 1980; Pinkerton and Wilson, 1994; Harris and Rowland, 2009). We are unable to measure the instantaneous effusion rate, however we can estimate the time-averaged discharge rate (TADR) for each flow, which is the total volume of the flow divided by the time over which it was emplaced (Harris et al., 2007). Due to temporal aliasing from the SAR acquisition interval, we do not know the exact start or end date for most flows, however we can use the earliest and latest possible start dates to provide a minimum bound on TADR for each flow (Fig. 9). From Arnold et al. (2017), we also have an estimate of the best fitting continuous discharge rate (red line in Fig. 9). However, this rate is based on the total erupted volume over 4.5 years, rather than the volume and eruption time of individual flows, and therefore underestimates the minimum rate for several flows.

There is no significant trend in the minimum TADR with time (the best fitting linear trend has a correlation coefficient $R^2 = 0.04$), however the long-term TADR shows an exponential decay with time (Arnold et al., 2017). Observations of lava

Table 3
Dimensions and yield strength of El Reventador lava flows.

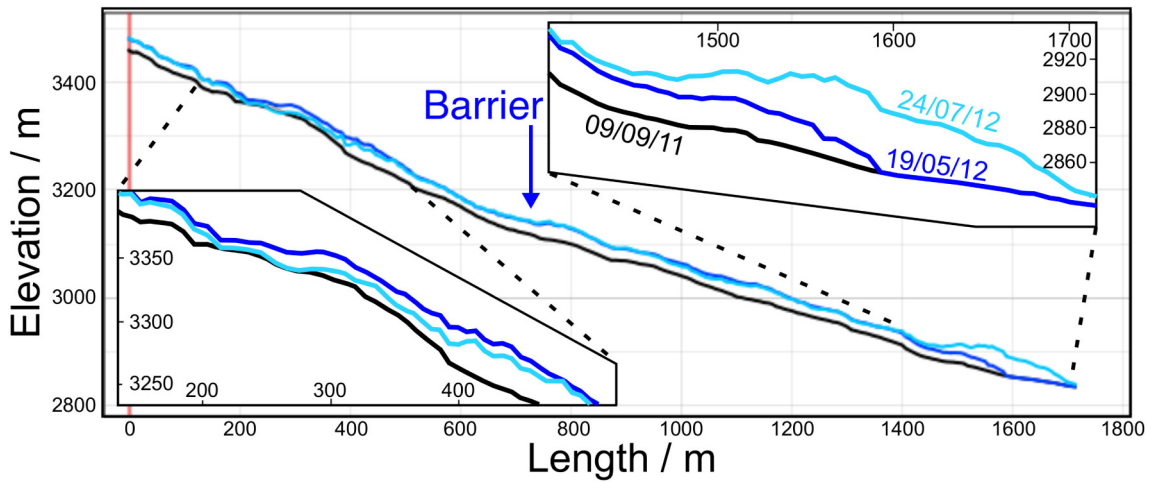| Flow	N	Thickness m	Levée width m	Flow width m	Slope °	Yield strength/kPa		
						Thickness method	Levée width method	Flow width method
19	36	17.6 ± 5.1	39.4 ± 9.1	161 ± 67	19.9 ± 7.7	120 ± 35	176 ± 40	45 ± 23
25	18	6.8 ± 2.2	20.5 ± 2.8	125 ± 22	26.1 ± 8.0	62 ± 20	168 ± 23	8 ± 4
28	16	7.1 ± 3.0	20.5 ± 1.3	128 ± 17	23.1 ± 4.0	55 ± 24	126 ± 13	9 ± 9
38	4	11.3 ± 0.9	24.8 ± 2.2	111 ± 8	28.9 ± 2.0	109 ± 8	232 ± 20	23 ± 4

Fig. 4. Downflow profile of Flow 19, taken along the centre line shown in Fig. 2a. The black line gives pre-Phase E topography on 9 September 2011, the dark blue lines give topography on 19 May 2012, when Flow 18 had been completely extruded and Flow 19 was still active, and light blue lines show topography on 24 July 2012, when Flow 19 had been completely emplaced. The blue arrow indicates the location where the flow starts to interact with the topographic barrier.

flows in previous phases of activity at El Reventador found that flows had higher TADR at the start of eruptive phases (Naranjo et al., 2016), which is similar to the long-term trend observed for Phase E. It is therefore likely that at least part of the observed decrease in flow length is due to decreasing TADR although changes in lava composition, crystallinity and volatile content are likely

to have an effect (e.g. Harris et al., 2007; Cashman and Sparks, 2013).

Due to the unconstrained nature of the TADR estimates, we do not find much correlation between TADR and flow parameters. However, there does appear to be a minimum threshold that constrains minimum flow length, area and volume (Fig. 10). These limits agree with
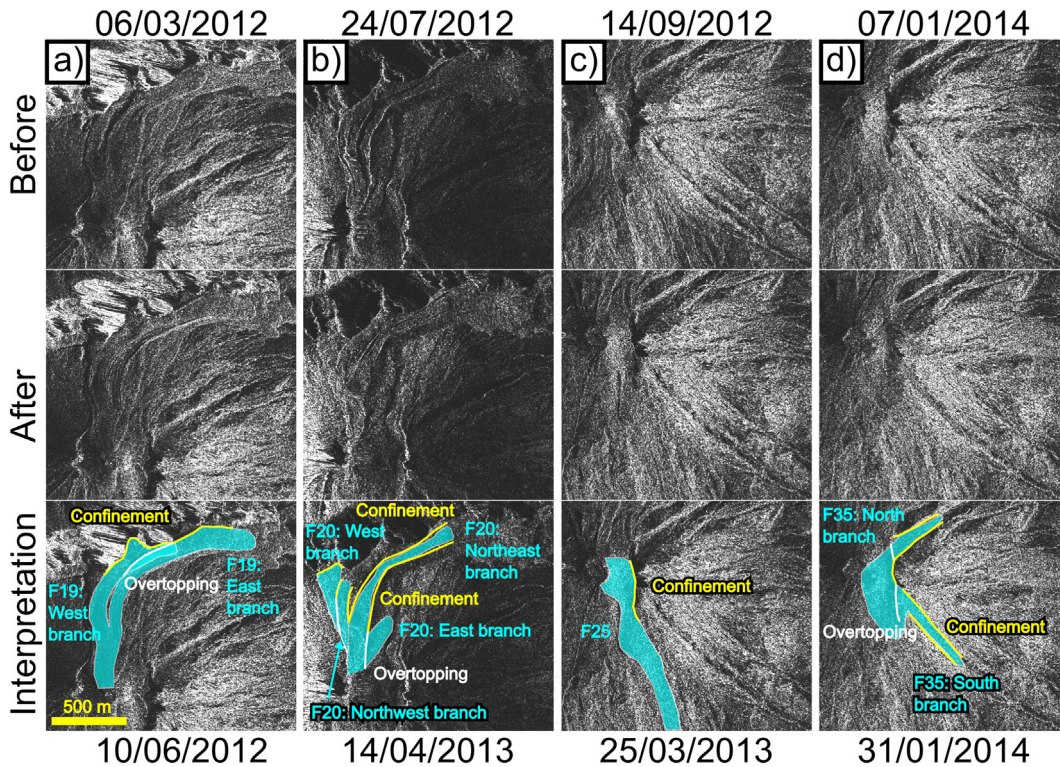
Fig. 5. Examples of interactions between lava flows and topographic barriers. Solid yellow lines show topographic barriers that are confining or diverting lava flows. Solid white lines show topographic barriers that have been overtopped by lava flows. a) Flow 19 was diverted to the northeast by the north crater wall, with the west branch also confined by the east branch. The west branch thickened until it overtopped the west levée of the eastern branch. b) The northeastern and northwestern branches of Flow 20 were confined on both sides by the levées of the eastern branch of Flow 19, while the eastern and western branches overtopped the levées. c) Flow 25 initially travelled east, but was diverted to the south by the eastern wall of the 2002 summit crater. d) Flow 35 impacted with the walls of the 2002 summit crater, and overtopped it to the north and south. These two branches of the flow advanced down fluvial gullies, which prevented lateral spreading.
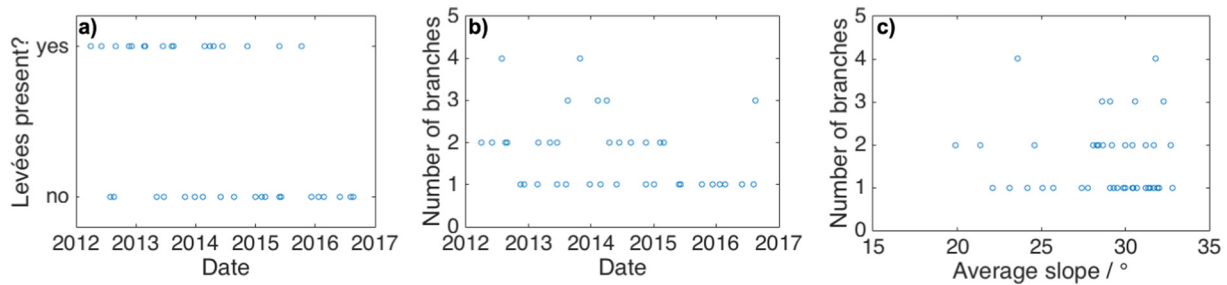
Fig. 6. Trend in a) presence or absence of levées, b) number of branches of El Reventador lava flows with time and c) number of branches with average underlying slope.

observations from basaltic flows on Hawai' i that for a given minimum TADR, there is an upper and lower bound to the length of lava flows (Walker et al., 1973; Malin, 1980; Pinkerton and Wilson, 1994). It is worth pointing out that Flow 37 appears to have an anomalously high minimum TADR (Fig. 10) mostly as a result of fortuitously timed satellite image acquisitions, which constrains the flow emplacement duration to within 24 days — a shorter maximum possible eruption duration than we can determine for other similarly sized flows. We discuss the impact of temporal aliasing on TADR measurements in Section 4.2.

If instead we plot flow dimensions against the long-term exponentially decaying effusion rate derived in Arnold et al. (2017) (red line in Fig. 9), then we find a slight correlation with flow length (Fig. 10e, $R^2 = 0.33$) and a stronger correlation with flow area (Fig. 10f $R^2 = 0.43$). The modelled eruption rate does not represent the instantaneous effusion rate or the time-averaged discharge rate (TADR) for the period the flows were active, and therefore (unlike these short-term rates) the long-term eruption rate should not have a direct impact on flow length. The significance of the observed correlations are discussed further in the next section.

4. Discussion

4.1. Influence of the conduit

The cumulative erupted volume of Phase E can be well fit by a smooth exponential or pseudo-exponential curve (Arnold et al., 2017). In order to generate a smooth long-term eruption rate curve, the frequency at which flows are emplaced must be greater than the average satellite repeat time, and there must be an approximately regular interval between flow emplacement, or else the cumulative volume curve (Fig. 6 in Arnold et al. (2017)) would appear 'stepped'. The extreme end-members of this emplacement behaviour would be

either constant lava extrusion at the long-term eruption rate (e.g. Kīlaueau, Hawai' i; Poland, 2014), or a long period of repose followed by the eruption of the total lava volume as one large flow at a higher rate, which has been observed at the andesitic eruptions of Lonquimay, Chile and Collier Cone, Oregon (Naranjo et al., 1992; Deardorff and Cashman, 2012). This second end-member would have significant hazard implications at El Reventador, since at both Longquimay and Collier Cone the eruptions generated a single long flow of 0.1 –0.2 km³ DRE that extended over 10 km from the eruption vent. Lava extrusion at these long andesitic flows was either observed (Lonquimay) or modelled (Collier Cone) to have taken place in under a year at average rates between 10 and 50 m³s⁻¹. The summit of El Reventador is approximately 8 km uphill of vital infrastructure, including a state highway and oil pipeline that would likely be buried and damaged or destroyed if the cumulative extrusive volume since 2002 had been erupted as a single flow at similar eruption rates.

The observed behaviour at El Reventador falls between the two proposed end-members of constant low-rate extrusion and eruption in a single large flow. We suggest the reason for the observed behaviour is temporary magma storage within the conduit in the mid to upper crust. Deformation observations and modelling presented by Arnold et al. (2017) indicate that the most likely conduit geometry is a ∼ north-south oriented dyke that extends from the summit vent down to a magma reservoir at ∼ 8 km depth. Observations of pulsed eruptions at Soufrière Hills Volcano, Montserrat and Bagana, Papua New Guinea have both been suggested as indications that a dyke-like conduit is acting as a capacitor (Costa et al., 2007; Wadge et al., 2012). This dyke capacitor temporarily stores magma as it ascends from the reservoir, until a threshold is exceeded, upon which the lava discharge rate increases. At Soufrière Hills and Bagana this results in pulses of increased activity with inter-pulse periods of several weeks, similar to the repeat frequency of individual lava flows at El Reventador. While we do not have exact constraints on the start dates of lava extrusion for most flows, if we average the number of flows erupted
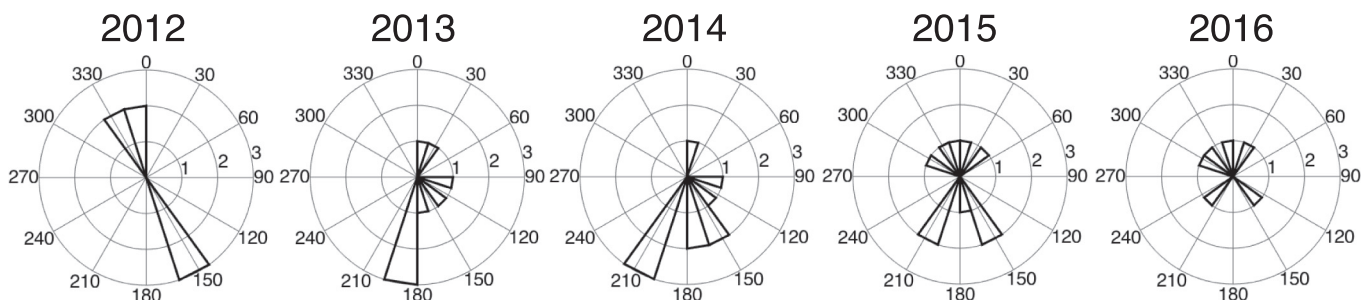

Fig. 7. Rose plots showing the initial direction of lava flow advance away from the summit lava dome by year. Radius indicates number of flows in the corresponding directional bin.
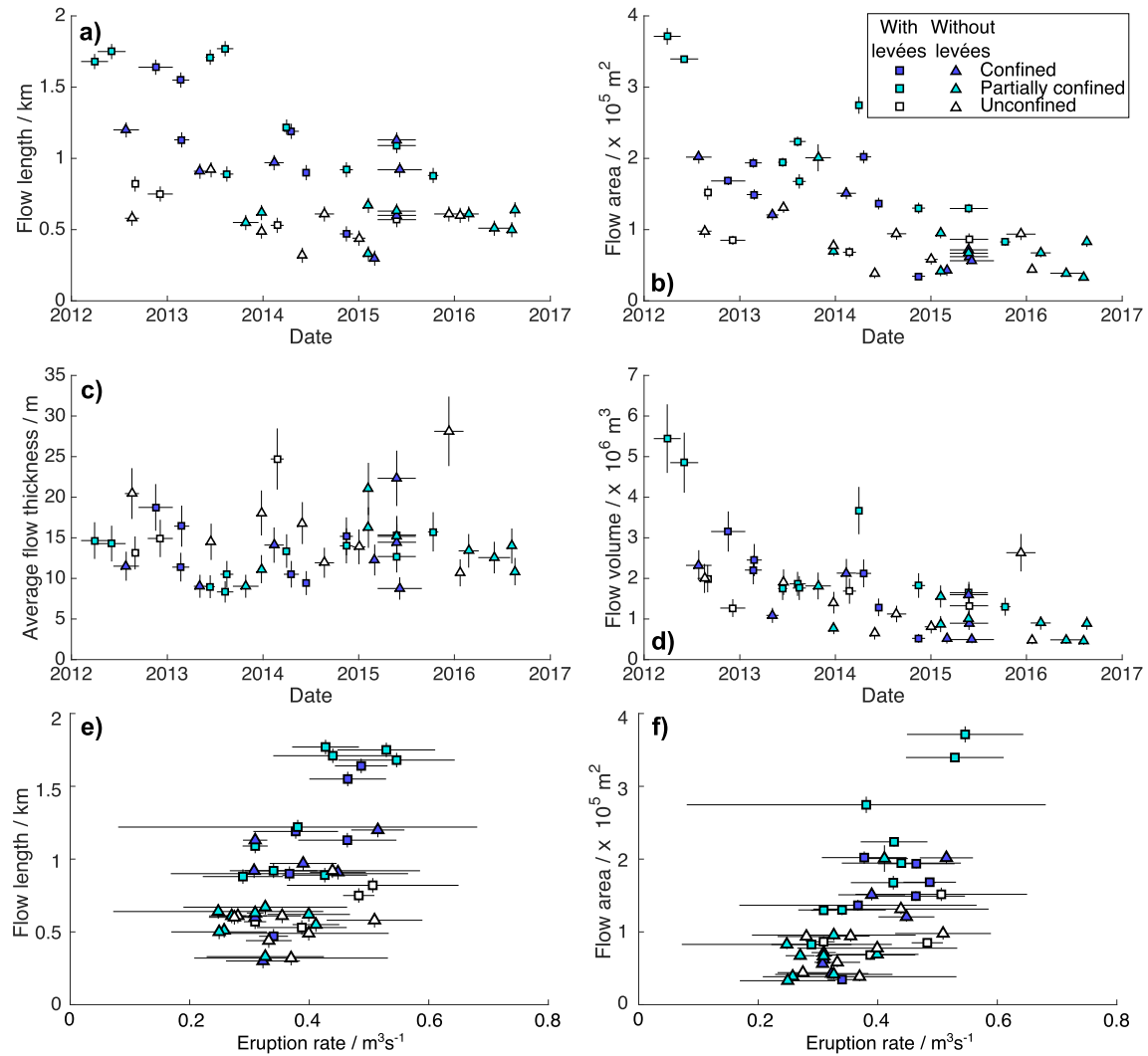
Fig. 8. Variation of lava flow dimensions with time and eruption rate. The errorbars indicate the maximum possible date range during which the flow could have been emplaced. a) Maximum flow length measured along centre of each flow with time. b) Area covered by each flow once flow advance stopped with time. c) Average flow thickness, estimated from multiple radar shadow measurements at the edge of each flow with time. d) Flow volume, calculated by multiplying flow area by average flow thickness with time. e) Maximum flow length measured along centre of each flow against eruption rate. f) Area covered by each flow once flow advance stopped against eruption rate. In each plot, squares represent flows that developed levées and triangles represent unchannelised flows. White symbols represent flows that were not laterally confined by topography, cyan symbols show flows that were confined on one side of the flow, and blue symbols indicate flows that were laterally confined on both sides.

over 6 month windows (a longer time period than the repeat interval of our SAR data), we find that the frequency of flow extrusion is approximately constant during the first 4.5 years of Phase E, with an average repose interval of 39 ± 32 days between the starts of flow extrusion.

The approximately constant repose interval despite the decreases in long-term eruption rate and flow volume (Fig. 8, Arnold et al. (2017)) indicates that the dyke capacitor is storing magma supplied from the reservoir for an approximately constant time interval before eruption. As the rate of magma supply for the reservoir decreases, the volume of the batches of magma stored in the dyke decreases, resulting in lower flow volumes. It is therefore likely that the flows at El Reventador are volume limited (e.g. Harris et al., 2007), and that the maximum length of flows is limited by the volume of batches of magma stored by the conduit.

The decay in effusion rate has potential to be used as an indicator of the end of an eruption (Bonny and Wright, 2017). However, effusion rate can be challenging to measure and this study suggests that flow length could be used as a proxy for systems such as Reventador where this correlation can be established.

Further evidence for the conduit exerting a control on the flow size and timing comes from the ground deformation episode presented by Arnold et al. (2017). The only magmatic ground deformation observed during Phase E occurred between March and June 2012, after the extrusion of Flow 18 but potentially coincident with the eruption of Flow 19. Flow 18 is the only flow out of the 43 observed that must have been emplaced over a period of longer than one month, and all later flows could have been emplaced more rapidly. The conduit opening event observed may have changed the capacitance of the dyke such that subsequently, magma temporarily stored in the conduit was released over a shorter duration. It is likely that the orientation of the dyke conduit also had an impact on the initial direction of flow travel, with most flows initially descending either the north or south flank of the summit lava dome.
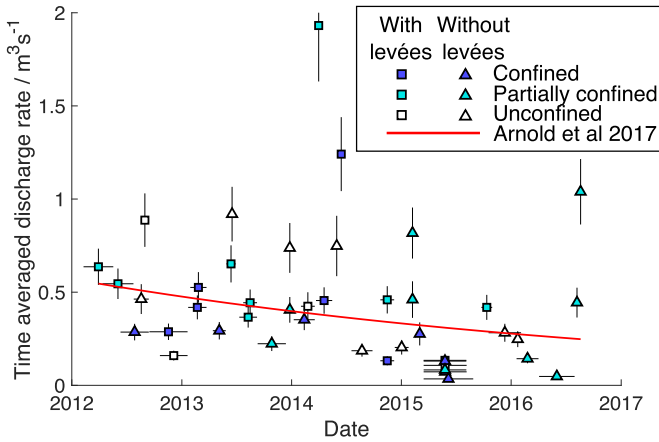
Fig. 9. Change in minimum time-averaged discharge rate with time. Solid red line indicates the best fitting exponential rate, derived from the cumulative erupted volume (Arnold et al., 2017). See Fig. 8 for explanation of other symbols.

4.2. Limitations of SAR for measuring flow properties

Theoretical and computational models exist to predict lava flow advance rate and geometry, based on trade-offs between advection and thermal diffusion derived from analogue models (e.g. Hulme, 1974; Huppert et al., 1982; Griffiths and Fink, 1993; Lyman and Kerr, 2006; Kerr et al., 2006; Dietterich et al., 2015; Garel et al., 2012). In order to apply these models to interpret lava flows, assumptions

have to be made about the material properties and rheology of the flows (e.g. Kerr and Lyman, 2007; Deardorff and Cashman, 2012; Castruccio et al., 2014; Dietterich et al., 2017). At El Reventador, we are limited in how well we can apply these models due to a lack of constraints on flow emplacement duration due to temporal aliasing as a result of the satellite revisit interval. Estimates of flow viscosity and rheology require knowledge of the flow velocity, and for most flows we only have a lower bound (Supplementary Material). Similarly, while we can put minimum constraints on the time-averaged discharge rate for each flow, estimating a realistic lava flux from flow dimensions requires knowledge of the flow rheology (e.g. Kerr et al., 2006; Deardorff and Cashman, 2012; Cashman et al., 2013; Castruccio et al., 2014).

The main limiting factor preventing further analysis of the data is therefore the lack of constraint on flow duration. Flows 18, 19 and 20, were emplaced over a longer duration than the satellite repeat interval, and we are therefore able to put minimum and maximum constraints on the time period over which these flows were emplaced (62–99 days, 24–103 days, and 26–94 days respectively). However there is still a significant uncertainty between the minimum and maximum emplacement durations for these flows, and for all other flows, the minimum duration is completely unconstrained.

Although the maximum and minimum emplacement durations are only loosely constrained for flows emplaced during Phase E, during Phases A–D, most flows were emplaced over time intervals between 3 and 12 days (Naranjo et al., 2016). Given flows that erupted during 2012 were petrologically similar to flows that erupted between 2002 and 2009, and fall within the range of dimensions of those flows (Naranjo, 2013; Naranjo et al., 2016), it is likely
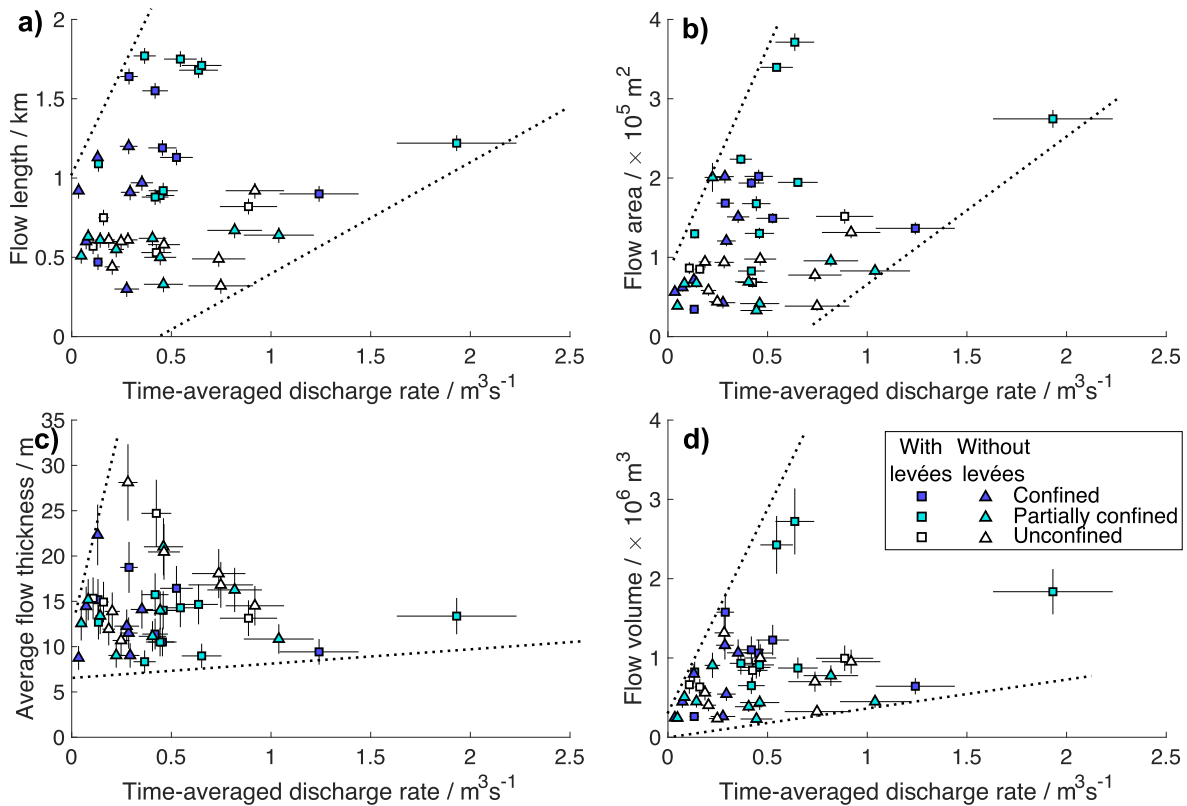

Fig. 10. Variation of lava flow dimensions with time-averaged and modelled discharge rates. Time-averaged rates (a–d) are minimum rates, estimated by dividing the flow volume by the maximum emplacement duration for each flow. Modelled discharge rates (e–f) are long-term average rates, derived from the best fitting exponential curve to the cumulative erupted volume presented by Arnold et al. (2017). a,e) Maximum flow length measured along centre of each flow. b,f) Area covered by each flow once flow advance stopped. c) Average flow thickness, estimated from multiple radar shadow measurements at the edge of each flow. d) Flow volume, calculated by multiplying flow area by average flow thickness. Black dotted lines indicate approximate linear bounds on observed values for a given minimum discharge rate. See Fig. 8 for explanation of other symbols.

that the emplacement duration for the Phase E flows (not including Flow 18) is similarly on the order of a few days to a few weeks. This conclusion is supported by infrared camera observations that Flow 38 was completely emplaced within 6 days (Vallejo Vargas et al., 2015), in contrast to our observations, which only require that the flow was emplaced in fewer than 54 days. The actual time-averaged discharge rate (TADR) supported by the infrared camera data for Flow 38 was therefore $4.24 \pm 0.66\,m^3s^{-1}$, an order of magnitude higher than our minimum estimate of $0.45 \pm 0.07\,m^3s^{-1}$ for the same flow. If we assume that all flows were emplaced in 6 days, then the bulk TADR for flow emplacement varies between 0.9 and $7.3\,m^3s^{-1}$. These TADR estimates are all significantly higher than the bulk long-term eruption rate of $0.35\,m^3s^{-1}$ that was calculated in Arnold et al. (2017).

5. Conclusions

In this study, we have combined satellite radar amplitude maps of lava flow extent and radar phase measurements of topographic change to investigate flow parameters and how these parameters varied over Phase E of the post-2002 eruption of El Reventador, Ecuador between 9 February 2012 and 24 August 2016. We mapped 43 distinct blocky andesitic lava flows that were erupted from a summit lava dome and primarily descended the north and south flanks of El Reventador through the breached north and south walls of a summit crater formed in the 3 November 2002 paroxysmal eruption.

We find that flows erupted during Phase E exhibit a range of features typical of andesitic flows, including levées and multiple branches. For over half the flows, interaction with pre-existing topographic barriers had some influence of the direction and lateral extent of the flows. The flow length, area and volume all decrease over the duration of the eruptive phase, as did the long-term eruption rate. Due to a lack of constraints on the flow emplacement times, we find little correlation between flux estimate and flow dimensions, however there appear to be upper and lower bounds on flow dimensions for a given minimum time-averaged discharge rate. The volume, emplacement duration, and frequency of flows were likely controlled by the dyke-like conduit acting as a magma capacitor and generating pulsed activity with a period of several weeks. This capacitance determines the maximum extrusion rate and length of erupted lava flows at El Reventador, limiting the hazard posed to local infrastructure. However, understanding the controls and limits of flow behaviours is important for understanding and mitigating against the potential hazard from andesitic lava flows at other, less remote, volcanic systems.

Large datasets for eruptive sequences containing multiple flows are rare, and largely limited to Hawai' i and Etna where flow dimensions and behaviour have been studied in great detail (e.g. Walker et al., 1973; Wadge, 1978; Malin, 1980; Pinkerton and Wilson, 1994; Calvari and Pinkerton, 1998; Harris et al., 2007; Harris and Rowland, 2009; Cashman et al., 2013). The dataset presented here describes 43 flows at Reventador volcano with similar physicals properties, but with varying volumes, degrees of confinement and interactions with obstacles providing a valuable resource for investigating the controls on flow behaviour. In particular, we describe natural examples of the types of dynamic interactions with topography suggested by analogue modelling (Dietterich et al., 2015). Furthermore, andesitic flows represent a significant but understudied hazard for large populations globally and our observations can be used to understand to what extent models of basaltic flows derived from Hawai' i and Etna can be extrapolated to predict the behaviour of andesitic flows. We observe some properties common to both basalt and andesites, for instance, confinement affects flow length both in Reventador and Hawai' i, despite the difference in composition. However, slope has little effect on the branching of the andesitic flows, probably due to the greater flow thickness and viscosity. The next step will be to apply existing lava flow models to the observations reported here to investigate the underlying rheological parameters, and improve hazard mapping of andesitic flows based on flow path and effusion rate.

Appendix A. Supplementary data

Supplementary data to this article can be found online at https://doi.org/10.1016/j.jvolgeores.2019.01.009.

References

Albino, F., Smets, B., D'Oreye, N., Kervyn, F., 2015. High-resolution TanDEM-X DEM: an accurate method to estimate lava flow volumes at Nyamulagira Volcano (D. R. Congo). J. Geophys. Res. Solid Earth 120, 4189–4207. https://doi.org/10.1002/2015JB011988.

Arnold, D.W.D., Biggs, J., Anderson, K., Vallejo Vargas, S., Wadge, G., Ebmeier, S.K., Naranjo, M.F., Mothes, P., 2017. Decaying lava extrusion rate at El Reventador Volcano, Ecuador, measured using high-resolution satellite radar. J. Geophys. Res. Solid Earth 122, https://doi.org/10.1002/2017JB014580.

Arnold, D.W.D., Biggs, J., Wadge, G., Ebmeier, S.K., Odbert, H.M., Poland, M.P., 2016. Dome growth, collapse, and valley fill at Soufrière Hills Volcano, Montserrat, from 1995 to 2013: contributions from satellite radar measurements of topographic change. Geosphere 12, 1300–1315. http://geosphere.gsapubs.org/lookup/doi/10.1130/GES01291.1. https://doi.org/10.1130/GES01291.1.

Bailey, J.E., Harris, A.J., Dehn, J., Calvari, S., Rowland, S.K., 2006. The changing morphology of an open lava channel on Mt. Etna. Bull. Volcanol. 68, 497–515. http://link.springer.com/10.1007/s00445-005-0025-6. https://doi.org/10.1007/s00445-005-0025-6.

Baldi, P., Fabris, M., Marsella, M., Monticelli, R., 2005. Monitoring the morphological evolution of the Sciara del Fuoco during the 2002–2003 Stromboli eruption using multi-temporal photogrammetry. ISPRS J. Photogramm. Remote Sens. 59, 199–211. http://www.sciencedirect.com/science/article/pii/S0924271605000079. https://doi.org/10.1016/j.isprsjprs.2005.02.004.

Behncke, B., Neri, M., Nagay, A., 2005. Lava flow hazard at Mount Etna (Italy): new data from a GIS-based study. Spec. Pap. 396 Kinemat. Dyn. lava flows. vol. 396. Geological Society of America, pp. 189–208. http://specialpapers.gsapubs.org/cgi/doi/10.1130/0-8137-2396-5.189. https://doi.org/10.1130/0-8137-2396-5.189.

Biggs, J., Pritchard, M.E., 2017. Global volcano monitoring: what does it mean when volcanoes deform? Elements 13, 17–22. http://elements.geoscienceworld.org/content/13/1/17. https://doi.org/10.2113/gselements.13.1.17.

Bonny, E., Wright, R., 2017. Predicting the end of lava flow-forming eruptions from space. Bull. Volcanol. 79, 52.

Borgia, A., Linneman, S., Spencer, D., Morales, L.D., Andre, J.B., 1983. Dynamics of lava flow fronts, Arenal Volcano, Costa Rica. J. Volcanol. Geotherm. Res. 19, 303–329.

Calvari, S., Pinkerton, H., 1998. Formation of lava tubes and extensive flow field during the 1991–1993 eruption of Mount Etna. J. Geophys. Res. 103301, 291-227. http://doi.wiley.com/10.1029/97JB03388. https://doi.org/10.1029/97JB03388.

Cashman, K.V., Soule, S.A., Mackey, B.H., Deligne, N.I., Deardorff, N.D., Dietterich, H.R., 2013. How lava flows: new insights from applications of lidar technologies to lava flow studies. Geosphere 9, 1664–1680. http://geosphere.gsapubs.org/content/9/6/1664.short. https://doi.org/10.1130/GES00706.1.

Cashman, K.V., Sparks, R.S.J., 2013. How volcanoes work: a 25 year perspective. Geol. Soc. Am. Bull. 125, 664–690. http://gsabulletin.gsapubs.org/content/125/5-6/664.full. https://doi.org/10.1130/B30720.1.

Castruccio, A., Rust, A.C., Sparks, R.S.J., 2013. Evolution of crust- and core-dominated lava flows using scaling analysis. Bull. Volcanol. 75, 1–15. http://link.springer.com/10.1007/s00445-012-0681-2. https://doi.org/10.1007/s00445-012-0681-2.

Castruccio, A., Rust, A.C., Sparks, R.S.J., 2014. Assessing lava flow evolution from post-eruption field data using Herschel-Bulkley rheology. J. Volcanol. Geotherm. Res. 275, 71–84. http://www.sciencedirect.com/science/article/pii/S0377027314000432. https://doi.org/10.1016/j.jvolgeores.2014.02.004.

Chevrel, M.O., Platz, T., Hauber, E., Baratoux, D., Lavallée, Y., Dingwell, D.B., 2013. Lava flow rheology: a comparison of morphological and petrological methods. Earth Planet. Sci. Lett. 384, 109–120. http://linkinghub.elsevier.com/retrieve/pii/S0012821X13005335. https://doi.org/10.1016/j.epsl.2013.09.022.

Chevrel, M.O., Siebe, C., Guilbaud, M.-N., Salinas, S., 2016. The AD 1250 El Metate shield volcano (Michoacán): Mexico's most voluminous holocene eruption and its significance for archaeology and hazards. Holocene 26, 471–488.

Cigolini, C., Borgia, A., Casertano, L., 1984. Intra-crater activity, aa-block lava, viscosity and flow dynamics: Arenal Volcano, Costa Rica. J. Volcanol. Geotherm. Res. 20, 155–176. http://linkinghub.elsevier.com/retrieve/pii/0377027384900726. https://doi.org/10.1016/0377-0273(84)90072-6.

Costa, A., Melnik, O., Sparks, R.S.J., Voight, B., 2007. Control of magma flow in dykes on cyclic lava dome extrusion. Geophys. Res. Lett. 34, L02303. http://doi.wiley.com/10.1029/2006GL027466. https://doi.org/10.1029/2006GL027466.

Deardorff, N.D., Cashman, K.V., 2012. Emplacement conditions of the c. 1,600-year bp Collier Cone lava flow, Oregon: a LiDAR investigation. Bull. Volcanol. 74, 2051–2066. http://link.springer.com/10.1007/s00445-012-0650-9. https://doi.org/10.1007/s00445-012-0650-9.

Dietterich, H.R., Cashman, K.V., 2014. Channel networks within lava flows: formation, evolution, and implications for flow behavior. J. Geophys. Res. Earth Surf. 119, 1704–1724. http://doi.wiley.com/10.1002/2014JF003103. https://doi.org/10.1002/2014JF003103.

Dietterich, H.R., Cashman, K.V., Rust, A.C., Lev, E., 2015. Diverting lava flows in the lab. Nat. Geosci. 8, 494–496. https://doi.org/10.1038/ngeo2470.

Dietterich, H.R., Lev, E., Chen, J., Richardson, J.A., Cashman, K.V., 2017. Benchmarking computational fluid dynamics models of lava flow simulation for hazard assessment, forecasting, and risk management. J. Appl. Volcanol. 6, 9. http://appliedvolc.springeropen.com/articles/10.1186/s13617-017-0061-x. https://doi.org/10.1186/s13617-017-0061-x.

Dietterich, H.R., Poland, M.P., Schmidt, D.A., Cashman, K.V., Sherrod, D.R., Espinosa, A.T., 2012. Tracking lava flow emplacement on the east rift zone of Kilauea, Hawai'i, with synthetic aperture radar coherence. Geochem. Geophys. Geosyst. 13, Q05001. http://doi.wiley.com/10.1029/2011GC004016. https://doi.org/10.1029/2011GC004016.

Ebmeier, S., Biggs, J., Mather, T., Elliott, J., Wadge, G., Amelung, F., 2012. Measuring large topographic change with InSAR: lava thicknesses, extrusion rate and subsidence rate at Santiaguito volcano, Guatemala. Earth Planet. Sci. Lett. 335-336, 216–225. http://www.sciencedirect.com/science/article/pii/S0012821X1200194X. https://doi.org/10.1016/j.epsl.2012.04.027.

Eichelberger, J.C., Carrigan, C.R., Westrich, H.R., Price, R.H., 1986. Non-explosive silicic volcanism. Nature 323, 598–602. http://www.nature.com/doifinder/10.1038/323598a0. https://doi.org/10.1038/323598a0.

Farquharson, J., James, M., Tuffen, H., 2015. Examining rhyolite lava flow dynamics through photo-based 3d reconstructions of the 2011–2012 lava flowfield at cordón-caulle, chile. J. Volcanol. Geotherm. Res. 304, 336–348.

Favalli, M., Chirico, G.D., Papale, P., Pareschi, M.T., Boschi, E., 2009. Lava flow hazard at Nyiragongo volcano, D.R.C. Bull. Volcanol. 71, 363–374. http://link.springer.com/10.1007/s00445-008-0233-y. https://doi.org/10.1007/s00445-008-0233-y.

Favalli, M., Fornaciai, A., Mazzarini, F., Harris, A., Neri, M., Behncke, B., Pareschi, M.T., Tarquini, S., Boschi, E., 2010. Evolution of an active lava flow field using a multitemporal LIDAR acquisition. J. Geophys. Res. Solid Earth 115, B11203. http://doi.wiley.com/10.1029/2010JB007463. https://doi.org/10.1029/2010JB007463.

Favalli, M., Pareschi, M.T., Neri, A., Isola, I., 2005. Forecasting lava flow paths by a stochastic approach. Geophys. Res. Lett. 32, 1–4. http://doi.wiley.com/10.1029/2004GL021718. https://doi.org/10.1029/2004GL021718.

Felpeto, A., Araña, V., Ortiz, R., Astiz, M., García, A., 2001. Assessment and modelling of lava flow hazard on Lanzarote (Canary Islands). Nat. Hazards 23, 247–257. http://link.springer.com/10.1023/A:1011112330766. https://doi.org/10.1023/A:1011112330766.

Fink, J.H., Griffiths, R.W., 1992. A laboratory analog study of the surface morphology of lava flows extruded from point and line sources. J. Volcanol. Geotherm. Res. 54, 19–32. http://linkinghub.elsevier.com/retrieve/pii/037702739290112Q. https://doi.org/10.1016/0377-0273(92)90112-Q.

Fink, J.H., Griffiths, R.W., 1998. Morphology, eruption rates, and rheology of lava domes: insights from laboratory models. J. Geophys. Res. 103, 527. http://doi.wiley.com/10.1029/97JB02838. https://doi.org/10.1029/97JB02838.

Fink, J.H., et al. 1987. The Emplacement of Silicic Domes and Lava Flows. vol. 212. Geological Society of America.

Flynn, L.P., Mouginis-Mark, P.J., Horton, K.A., 1994. Distribution of thermal areas on an active lava flow field: Landsat observations of Kilauea, Hawaii, July 1991. Bull. Volcanol. 56, 284–296. http://link.springer.com/10.1007/BF00302081. https://doi.org/10.1007/BF00302081.

Garel, F., Kaminski, E., Tait, S., Limare, A., 2012. An experimental study of the surface thermal signature of hot subaerial isoviscous gravity currents: implications for thermal monitoring of lava flows and domes. J. Geophys. Res. Solid Earth 117.

Goitom, B., Oppenheimer, C., Hammond, J.O.S., Grandin, R., Barnie, T., Donovan, A., Ogubazghi, G., Yohannes, E., Kibrom, G., Kendall, J.-M., Carn, S.A., Fee, D., Sealing, C., Keir, D., Ayele, A., Blundy, J., Hamlyn, J., Wright, T., Berhe, S., 2015. First recorded eruption of Nabro volcano, Eritrea, 2011. Bull. Volcanol. 77, 85. http://link.springer.com/10.1007/s00445-015-0966-3. https://doi.org/10.1007/s00445-015-0966-3.

Gregg, T.K.P., Fink, J.H., 2000. A laboratory investigation into the effects of slope on lava flow morphology. J. Volcanol. Geotherm. Res. 96, 145–159. http://www.sciencedirect.com/science/article/pii/S0377027399001481. https://doi.org/10.1016/S0377-0273(99)00148-1.

Griffiths, R.W., Fink, J.H., 1993. Effects of surface cooling on the spreading of lava flows and domes. J. Fluid Mech. 252, 667–702. https://www.cambridge.org/core/journals/journal-of-fluid-mechanics/article/effects-of-surface-cooling-on-the-spreading-of-lava-flows-and-domes/63FA486D26D5D5F24E658C013511409E. https://doi.org/10.1017/S0022112093003933.

Harris, A., Rowland, S., 2009. Effusion rate controls on lava flow length and the role of heat loss: a review. Stud. Volcanol. Leg. Georg. Walker. Spec. Publ. IAVCEI 2. Geological Society, London, Bath, UK, pp. 33–51. (chapter 2). https://books.google.co.uk/books?hl=en&lr=&id=7-l_65bugsoC&oi=fnd&pg=PA33&ots=OL286FpIoW&sig=h6q2jBb2SStI8LPyuKMy4ajshoo.

Harris, A.J., Flynn, L.P., Matias, O., Rose, W.I., Cornejo, J., 2004. The evolution of an active silicic lava flow field: an ETM+ perspective. J. Volcanol. Geotherm. Res. 135, 147–168. http://www.sciencedirect.com/science/article/pii/S0377027304000356. https://doi.org/10.1016/j.jvolgeores.2003.12.011.

Harris, A.J.L., Dehn, J., Calvari, S., 2007. Lava effusion rate definition and measurement: a review. Bull. Volcanol. 70, 1–22. http://link.springer.com/10.1007/s00445-007-0120-y. https://doi.org/10.1007/s00445-007-0120-y.

Hulme, G., 1974. The interpretation of lava flow morphology. Geophys. J. R. Astron. Soc. 39, 361–383. https://academic.oup.com/gji/article-lookup/doi/10.1111/j.1365-246X.1974.tb05460.x. https://doi.org/10.1111/j.1365-246X.1974.tb05460.x.

Huppert, H.E., Shepherd, J.B., Haraldur Sigurdsson, R., Sparks, S.J., 1982. On lava dome growth, with application to the 1979 lava extrusion of the Soufrière of St. Vincent. J. Volcanol. Geotherm. Res. 14, 199–222. https://doi.org/10.1016/0377-0273(82)90062-2.

James, M.R., Robson, S., Pinkerton, H., Ball, M., 2006. Oblique photogrammetry with visible and thermal images of active lava flows. Bull. Volcanol. 69, 105–108. http://link.springer.com/10.1007/s00445-006-0062-9. https://doi.org/10.1007/s00445-006-0062-9.

Jenkins, S.F., Day, S.J., Faria, B.V.E., Fonseca, J.F.B.D., 2017. Damage from lava flows: insights from the 2014–2015 eruption of Fogo, Cape Verde. J. Appl. Volcanol. 6, 6. http://appliedvolc.springeropen.com/articles/10.1186/s13617-017-0057-6. https://doi.org/10.1186/s13617-017-0057-6.

Kelfoun, K., Vallejo Vargas, S., 2015. VolcFlow capabilities and potential development for the simulation of lava flows. Geol. Soc. London, Spec. Publ. 426, SP426.8. http://sp.lyellcollection.org/lookup/doi/10.1144/SP426.8. https://doi.org/10.1144/SP426.8.

Kereszturi, G., Németh, K., Moufti, M.R., Cappello, A., Murcia, H., Ganci, G., Del Negro, C., Procter, J., Zahran, H.M.A., 2016. Emplacement conditions of the 1256 AD Al-Madinah lava flow field in Harrat Rahat, Kingdom of Saudi Arabia - insights from surface morphology and lava flow simulations. J. Volcanol. Geotherm. Res. 309, 14–30. http://www.sciencedirect.com/science/article/pii/S0377027315003686. https://doi.org/10.1016/j.jvolgeores.2015.11.002.

Kerr, R.C., Griffiths, R.W., Cashman, K.V., 2006. Formation of channelized lava flows on an unconfined slope. J. Geophys. Res. 111, B10206. http://doi.wiley.com/10.1029/2005JB004225. https://doi.org/10.1029/2005JB004225.

Kerr, R.C., Lyman, A.W., 2007. Importance of surface crust strength during the flow of the 1988–1990 andesite lava of Lonquimay Volcano, Chile. J. Geophys. Res. Solid Earth 112, B03209. http://doi.wiley.com/10.1029/2006JB004522. https://doi.org/10.1029/2006JB004522.

Kilburn, C.R., Lopes, R.M., 1991. General patterns of flow field growth: Aa and blocky lavas. J. Geophys. Res. Solid Earth 96, 19721–19732.

Kubanek, J., Richardson, J.A., Charbonnier, S.J., Connor, L.J., 2015,a. Lava flow mapping and volume calculations for the 2012–2013 Tolbachik, Kamchatka, fissure eruption using bistatic TanDEM-X InSAR. Bull. Volcanol. 77, 1–13. http://link.springer.com/10.1007/s00445-015-0989-9. https://doi.org/10.1007/s00445-015-0989-9.

Kubanek, J., Westerhaus, M., Schenk, A., Aisyah, N., Brotopuspito, K.S., Heck, B., 2015b. Volumetric change quantification of the 2010 Merapi eruption using TanDEM-X InSAR. Remote Sens. Environ. 164, 16–25. http://www.sciencedirect.com/science/article/pii/S0034425715000863. https://doi.org/10.1016/j.rse.2015.02.027.

Lipman, P.W., Banks, N.G., 1987. AA flow dynamics: Mauna Loa 1984. US Geol. Surv. Prof. Pap. 1350, 1527–1567. https://pubs.usgs.gov/pp/1987/1350/pdf/chapters/pp1350_ch57.pdf.

Lyman, A.W., Kerr, R.C., 2006. Effect of surface solidification on the emplacement of lava flows on a slope. J. Geophys. Res. Solid Earth 111, http://doi.wiley.com/10.1029/2005JB004133. https://doi.org/10.1029/2005JB004133. (n/a–n/a).

Lyman, A.W., Koenig, E., Fink, J.H., 2004. Predicting yield strengths and effusion rates of lava domes from morphology and underlying topography. J. Volcanol. Geotherm. Res. 129, 125–138.

Malin, M.C., 1980. Lengths of Hawaiian lava flows. http://geology.gsapubs.org/cgi/doi/10.1130/0091-7613(1980)8%3C306:LOHLF%3E2.0.CO;2. https://doi.org/10.1130/0091-7613(1980)8<306:LOHLF>2.0.CO;2.

Moore, H.J., Arthur, D.W., Schaber, G.G., 1978. Yield strengths of flows on the Earth, Mars, and moon. http://adsabs.harvard.edu/full/1978LPSC.9.3351M.

Naranjo, J.A., Sparks, R.S.J., Stasiuk, M.V., Moreno, H., Ablay, G.J., 1992. Morphological, structural and textural variations in the 1988–1990 andesite lava of Lonquimay volcano, Chile. Geol. Mag. 129, 657–678. http://journals.cambridge.org/article_S0016756800008426. https://doi.org/10.1017/S0016756800008426.

Naranjo, M.F., 2013. Estudio petro-geoquímico y cronológico de los flujos de lava emitidos por el volcán Reventador entre 2002 a 2009. Masters thesis. Escuela Politécnica Nacional. http://bibdigital.epn.edu.ec/handle/15000/6443.

Naranjo, M.F., Ebmeier, S.K., Vallejo, S., Ramón, P., Mothes, P., Biggs, J., Herrera, F., 2016. Mapping and measuring lava volumes from 2002 to 2009 at El Reventador Volcano, Ecuador, from field measurements and satellite remote sensing. J. Appl. Volcanol. 5, 8. http://appliedvolc.springeropen.com/articles/10.1186/s13617-016-0048-z. https://doi.org/10.1186/s13617-016-0048-z.

National Academies of Sciences Engineering and Medicine, 2017. Volcanic Eruptions and Their Repose, Unrest, Precursors, and Timing. National Academies Press, Washington, D.C.. https://www.nap.edu/catalog/24650. https://doi.org/10.17226/24650.

Navarro-Ochoa, C., Gavilanes-Ruíz, J.C., Cortés-Cortés, A., 2002. Movement and emplacement of lava flows at Volcán de Colima, México: November 1998–February 1999. J. Volcanol. Geotherm. Res. 117, 155–167. https://doi.org/10.1016/S0377-0273(02)00242-1.

Pinel, V., Poland, M., Hooper, A., 2014. Volcanology: lessons learned from synthetic aperture radar imagery. J. Volcanol. Geotherm. Res. 289, 81–113. http://www.sciencedirect.com/science/article/pii/S0377027314003084. https://doi.org/10.1016/j.jvolgeores.2014.10.010.

Pinkerton, H., Wilson, L., 1994. Factors controlling the lengths of channel-fed lava flows. Bull. Volcanol. 56, 108–120. http://link.springer.com/10.1007/BF00304106. https://doi.org/10.1007/BF00304106.

Poland, M.P., 2014. Time-averaged discharge rate of subaerial lava at Kilauea Volcano, Hawaii, measured from TanDEM-X interferometry: implications for magma supply and storage during 2011–2013. J. Geophys. Res. Solid Earth 119, 5464–5481. http://doi.wiley.com/10.1002/2014JB011132. https://doi.org/10.1002/2014JB011132.

Pyle, D.M., Elliott, J.R., 2006. Quantitative morphology, recent evolution, and future activity of the Kameni Islands volcano, Santorini, Greece. Geosphere 2, 253–268. http://geosphere.gsapubs.org/cgi/doi/10.1130/GES00028.1. https://doi.org/10.1130/GES00028.1.

Pyle, D.M., Mather, T.A., Biggs, J., 2013. Remote sensing of volcanoes and volcanic processes: integrating observation and modelling - introduction. Geol. Soc. London, Spec. Publ. 380, 1–13. http://sp.lyellcollection.org/content/380/1/1.full. https://doi.org/10.1144/SP380.14.

Ridolfi, F., Puerini, M., Renzulli, A., Menna, M., Toulkeridis, T., 2008. The magmatic feeding system of El Reventador volcano (Sub-Andean zone, Ecuador) constrained by texture, mineralogy and thermobarometry of the 2002 erupted products. J. Volcanol. Geotherm. Res. 176, 94–106. http://www.sciencedirect.com/science/article/pii/S0377027308000930. https://doi.org/10.1016/j.jvolgeores.2008.03.003.

Rumpf, M.E., Lev, E., Wysocki, R., 2018. The influence of topographic roughness on lava flow emplacement. Bull. Volcanol. 80, 63.

Samaniego, P., Eissen, J.P., Le Pennec, J.L., Robin, C., Hall, M.L., Mothes, P., Chavrit, D., Cotten, J., 2008. Pre-eruptive physical conditions of El Reventador volcano (Ecuador) inferred from the petrology of the 2002 and 2004–05 eruptions. J. Volcanol. Geotherm. Res. 176, 82–93. http://linkinghub.elsevier.com/retrieve/pii/S0377027308001005. https://doi.org/10.1016/j.jvolgeores.2008.03.004.

Simkin, T., Siebert, L., McClelland, L., Bridge, D., Newhall, C., Latter, J.H., 1981. Volcanoes of the World: A Regional Directory, Gazetteer, and Chronology of Volcanism during the Last 10,000 years. Hutchinson Ross Pub. Co., New York.

Smets, B., Wauthier, C., D'Oreye, N., 2010. A new map of the lava flow field of Nyamulagira (D.R. Congo) from satellite imagery. J. Afr. Earth Sci. 58, 778–786. http://www.sciencedirect.com/science/article/pii/S1464343X10001482. https://doi.org/10.1016/j.jafrearsci.2010.07.005.

Sparks, R.S.J., Biggs, J., Neuberg, J.W., 2012. Monitoring volcanoes. Science 335, 1310–1311. http://science.sciencemag.org/content/335/6074/1310. https://doi.org/10.1126/science.1219485. (80-.).

Sparks, R.S.J., Pinkerton, H., Hulme, G., 1976. Classification and formation of lava levees on Mount Etna, Sicily. Geology 4, 269–271. http://geology.gsapubs.org/cgi/doi/10.1130/0091-7613(1976)4%3C269:CAFOLL%3E2.0.CO;2. https://doi.org/10.1130/0091-7613(1976)4<269:CAFOLL>2.0.CO;2.

Tarquini, S., Vitturi, M. d., 2014. Influence of fluctuating supply on the emplacement dynamics of channelized lava flows. Bull. Volcanol. 76, 801.

Vallejo Vargas, S., Kelfoun, K., Diefenback, A., Ramón, P., Vasconez, F., Naranjo, M.F., Pino, G., 2015. Numerical simulations of lava flows. A calibration from thermal images of lava emplacement at El Reventador volcano. Int. Union Geol. Geophys. Gen. Assem., Prague. https://www.researchgate.net/publication/294729286_Vallejo_et_al_IUGG-2015.

Wadge, G., 1978. Effusion rate and the shape of aa lava flow-fields on Mount Etna. Geology 6, 503–506. http://geology.gsapubs.org/cgi/doi/10.1130/0091-7613(1978)6%3C503:ERATSO%3E2.0.CO;2. https://doi.org/10.1130/0091-7613(1978)6<503:ERATSO>2.0.CO;2.

Wadge, G., 1981. The variation of magma discharge during basaltic eruptions. J. Volcanol. Geotherm. Res. 11, 139–168. https://doi.org/10.1016/0377-0273(81)90020-2.

Wadge, G., Cole, P., Stinton, A., Komorowski, J.-C., Stewart, R., Toombs, A., Legendre, Y., 2011. Rapid topographic change measured by high-resolution satellite radar at Soufriere Hills Volcano, Montserrat. J. Volcanol. Geotherm. Res. 199, 142–152. http://www.sciencedirect.com/science/article/pii/S0377027310003434. https://doi.org/10.1016/j.jvolgeores.2010.10.011.

Wadge, G., Odbert, H., Macfarlane, D., James, M., 2006. The November 2005 DEM of the Soufrière Hills Crater. Montserrat Volcano Obs. …. https://scholar.google.co.uk/scholar?hl=en&q=The+November+2005+DEM+of+the+Soufriere+Hills+crater&btnG=&as_sdt=1%2C5&as_sdtp=#0.

Wadge, G., Saunders, S., Itikarai, I., 2012. Pulsatory andesite lava flow at Bagana Volcano. Geochem. Geophys. Geosyst. 13, http://doi.wiley.com/10.1029/2012GC004336. https://doi.org/10.1029/2012GC004336. (n/a–n/a).

Wadge, G., Voight, B., Sparks, R.S.J., Cole, P.D., Loughlin, S.C., Robertson, R.E.A., 2014. Chapter 1 An overview of the eruption of Soufriere Hills Volcano, Montserrat from 2000 to 2010. Geol. Soc. Lond. Mem. 39, 1–40. http://mem.lyellcollection.org/content/39/1/1.full. https://doi.org/10.1144/M39.1.

Walker, G.P.L., Huntingdon, A.T., Sanders, A.T., Dinsdale, J.L., 1973. Lengths of lava flows [and discussion]. Philos. Trans. R. Soc. A Math. Phys. Eng. Sci. 274, 107–118. http://rsta.royalsocietypublishing.org/content/274/1238/107. https://doi.org/10.1098/rsta.1973.0030.

Werner, C., Wegmüller, U., Strozzi, T., Wiesmann, A., 2000. Gamma SAR and interferometric processing software. Proc. ERS-Envisat Symp. http://citeseerx.ist.psu.edu/viewdoc/download?doi=10.1.1.20.6363&rep=rep1&type=pdf.

Wright, R., 2016. MODVOLC: 14 years of autonomous observations of effusive volcanism from space. Geol. Soc. London, Spec. Publ. 426, 23–53. http://sp.lyellcollection.org/lookup/doi/10.1144/SP426.12. https://doi.org/10.1144/SP426.12.

Xu, W., Jónsson, S., 2014. The 2007–8 volcanic eruption on Jebel at Tair island (Red Sea) observed by satellite radar and optical images. Bull. Volcanol. 76, 795. http://link.springer.com/article/10.1007/s00445-014-0795-9/fulltext.html. https://doi.org/10.1007/s00445-014-0795-9.